



36 I. Introduction

37 The topological and conformational information provided by scalar couplings lies at the foundation of the
38 analytical power of NMR spectroscopy (Ernst et al., 1987; Keeler, 2005; Levitt, 2008; Cavanagh, 2007). The
39 strong coupling case is encountered when scalar coupling constants are not negligible with respect to the
40 difference of resonance frequency between the coupled spins (Keeler, 2005). Understanding strong scalar
41 couplings and their spectral signature was essential when NMR was introduced for chemical analysis,
42 which was typically performed at magnetic fields considered today as low (Bodenhausen et al., 1977;
43 Pfändler and Bodenhausen, 1987). Modern high-field NMR is widely based on the exploitation of weak
44 scalar couplings, so that strong scalar couplings have remained a nuisance, in particular in aromatic spin
45 systems (Vallurupalli et al., 2007; Foroozandeh et al., 2014). Recently, the development and availability of
46 benchtop NMR spectrometers operating at low or moderate magnetic fields (Grootveld et al., 2019), has
47 revived the interest in the understanding of strong scalar couplings in conventional NMR.

48 Contrarily to conventional NMR, NMR at near-zero or ultralow magnetic fields (ZULF-NMR), explores the
49 benefits of NMR in the strong scalar-coupling regime. At such magnetic fields, typically smaller than 1 μ T,
50 scalar coupling interactions dominate all Zeeman interaction and dictate the eigenstates of spin systems
51 and transition energies obtained in spectra (Ledbetter et al., 2011; Tayler et al., 2017; Blanchard and
52 Budker, 2016). However, for homonuclear couplings, the transition between the weak- and strong-
53 coupling regimes occurs in a range of magnetic fields, where the Zeeman interaction is still dominant
54 (Ivanov et al., 2006; Ivanov et al., 2008; Ivanov et al., 2014; Appelt et al., 2010). This transition between
55 weak and strong couplings can be investigated by varying the magnetic field applied to the sample on a
56 high-field magnet, which is usually performed by moving the sample through the stray field with a shuttle
57 system (Roberts and Redfield, 2004b, a; Redfield, 2012; Wagner et al., 1999; Bryant and Korb, 2005;
58 Goddard et al., 2007; Chou et al., 2016; Chou et al., 2017; Charlier et al., 2013; Cousin et al., 2016a; Cousin
59 et al., 2016b; Zhukov et al., 2018; Kiryutin et al., 2016). These studies have highlighted the effects of level
60 anti-crossings (LACs) (Miesel et al., 2006; Ivanov et al., 2014). When the passage through a LAC is slow,
61 the transition is adiabatic and the population of eigenstates is smoothly converted to the new eigenstates.
62 When the transition is fast, coherences can be generated between the new eigenstates and time-
63 oscillations of the population of high-field eigenstates can be observed (Pravdivtsev et al., 2013; Kiryutin
64 et al., 2013). This phenomenon has been observed on a variety of homonuclear spin systems.
65 Heteronuclear scalar couplings have been shown to alter LACs in homonuclear spin systems (Korchak et
66 al., 2012); yet, the properties of such heteronuclear couplings on LACs are not fully understood, in
67 particular, in spin systems with extensive networks of homo- and heteronuclear scalar couplings.

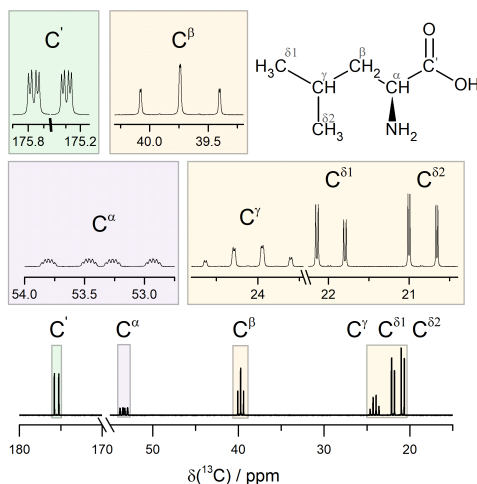
68 Here, we investigate the effect of heteronuclear scalar couplings on LACs in a spin system typical of
69 biomolecular NMR, a uniformly carbon-13 labeled amino acid (leucine), which combines extensive
70 networks of homo- and heteronuclear scalar couplings. Essentially, we exploit the ability to apply
71 composite pulse decoupling on our two-field NMR spectrometer (Cousin et al., 2016a) to switch on and
72 off heteronuclear scalar couplings at low magnetic field. We demonstrate that heteronuclear scalar
73 couplings alter LACs by sustaining the weak-coupling regime in a carbon-13 homonuclear spin system.
74 Composite pulse decoupling at low magnetic field restores the strong scalar coupling regime in the
75 carbon-13 nuclei of the isopropyl group of leucine at 0.33 T. Our results identify how heteronuclear
76 couplings alter homonuclear couplings at low magnetic fields, which could be exploited in low-field NMR
77 methodology and may be considered in further developments of total correlation spectroscopy (TOCSY)
78 (Braunschweiler and Ernst, 1983) mixing sequences in high-field NMR.

79 II. Methods

80 A. Sample preparation



81 Experiments have been performed using the following sample: 76 mM 99% enriched $^{13}\text{C},^{15}\text{N}$ labeled L-
82 leucine (Leu) in 90% H_2O 10% D_2O solution. $^{13}\text{C},^{15}\text{N}$ enriched L-leucine were purchased from Sigma-Aldrich
83 and used as it stands. ^{13}C -NMR spectrum of the labelled Leu molecule is shown in **Figure 1**. We also show
84 separately the signals of the individual carbon nuclei. Broadband proton decoupling was used to simplify
85 the spectrum. Here, we will focus on a three-spin system, formed by the C^γ and two C^δ nuclei of the
86 isopropyl moiety. We will study polarization transfer in this subsystem upon fast switch of the external
87 magnetic field obtained by a transfer of the sample through the stray field of a high-field NMR magnet.



88

89 **Figure 1.** Structure of $^{13}\text{C},^{15}\text{N}$ L-leucine and 100.62 MHz ^{13}C -NMR spectrum under broadband ^1H decoupling. Signal
90 of each carbon nuclei is also shown separately. The multiplet structure in the spectrum is due to non-decoupled ^{13}C -
91 ^{13}C and ^{13}C - ^{15}N scalar interactions.

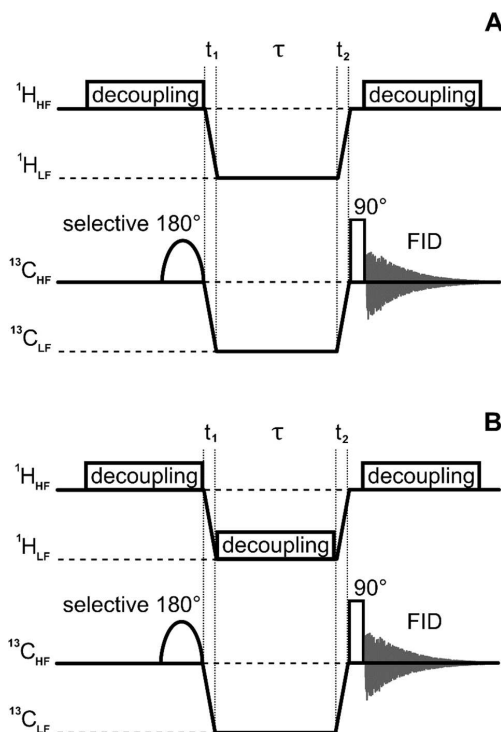
92 B. Field-cycling NMR experiments

93 NMR experiments were performed on a two-field NMR spectrometer (Cousin et al., 2016a) with fast
94 sample shuttling (Charlier et al., 2013). The high field $B_{HF} = 14.1$ T is the detection field of a 600 MHz
95 NMR spectrometer while the low field is $B_{LF} = 0.33$ T. The magnetic field in the low-field centre is
96 sufficiently homogeneous (inhomogeneities of the order of 10 ppm) so that radiofrequency (RF) pulses
97 can be applied by using a triple-resonance NMR probe, as described previously (Cousin et al., 2016a).

98 Field-cycling NMR experiments were run according to the pulse sequences depicted in **Figure 2**. First, a
99 non-equilibrium state is generated at B_{HF} by applying a selective NMR pulse (shaped ReBurp pulse (Geen
100 and Freeman, 1991)) to the $\text{C}^{\delta 2}$ nucleus (the pulse duration was 46.4 ms, the peak RF-field amplitude was
101 adjusted to cover *ca.* 100 Hz bandwidth around the center of $\text{C}^{\delta 2}$ signal). To improve the selectivity of the
102 pulse, simultaneous proton decoupling was used, which reduces multiplet overlay in the carbon-13 NMR
103 spectrum. Following this preparation, the sample was shuttled from the high-field center to the low-field
104 center $B_{HF} \rightarrow B_{LF}$ with a duration $t_1 = 110$ ms. The field jump is fast enough to be non-adiabatic and it
105 is aimed to excite a spin coherence. Subsequently, the coherence evolves at B_{LF} during a variable time
106 period τ . The shuttle transfer back to the high-field center leads to a second field jump $B_{LF} \rightarrow B_{HF}$ with a
107 duration $t_2 = 95$ ms. This second non-adiabatic field jump to B_{HF} converts the coherence into a
108 population difference. Detection is performed after a $\pi/2$ pulse on the carbon-13 channel in the presence
109 of proton decoupling. We perform two types of experiments, in which the carbon spin coherence (zero-
110 quantum coherence, ZQC) evolves at B_{LF} in the absence (see **Figure 2A**) and in the presence (see **Figure**
111 **2B**) of proton composite-pulse decoupling. Decoupling at B_{LF} has been performed using composite pulse
112 decoupling pulse with the WALTZ-64 supercycle (Shaka et al., 1983) at low field on the proton RF-channel
113 (operating at 14 MHz corresponding to the proton NMR frequency at 0.33 T). The τ -dependence of



114 polarization is expected to be oscillatory, due to the coherent polarization exchange within the expectedly
115 strongly coupled system of the C^γ and two C^δ carbon-13 nuclei.



116
117 **Figure 2.** Experimental protocols of field-cycling NMR experiments without ¹H decoupling at the low field (A) and
118 with 24 kHz WALTZ-64 ¹H decoupling at the low field (B). Details of the experiments: 0.56 W WALTZ-64 composite
119 pulse decoupling on the proton channel was applied at B_{HF} during 100 ms prior to a selective 180-degree pulse, in
120 order to enhance ¹³C polarization by the nuclear Overhauser effect. The sample shuttle times, t₁ and t₂, were 80 ms
121 and 120 ms, respectively. Selective inversion was performed with a ReBurb pulse (Geen and Freeman, 1991) with a
122 duration of 46.4 ms at the C^{δ2} resonant frequency covering ca. 100 Hz bandwidth. The delay τ at low field was varied
123 with a 5 ms step. After sample transfer to high field, a hard 90-degree pulse generated ¹³C transverse magnetization;
124 FID acquisition was done during 1.56 s under 2.7 kHz WALTZ-64 proton decoupling.

125 III. Theory

126 A. Polarization transfer in a 3-spin system

127 In this subsection, we provide a theoretical description of the field-cycling NMR experiments. First, we
128 present the analytical treatment of polarization transfer among two nuclei of the same kind, here spin I₁
129 and spin I₂ (e.g. two carbon-13 nuclei), in the presence of a third spin S, which can be a heteronucleus
130 (e.g. here a proton). This is the minimal system allowing us to detail the effect of a heteronucleus on
131 polarization transfer among strongly coupled spins. We assume that spins I₁ and I₂ are in strong coupling
132 conditions, meaning that the difference, δω, in their Zeeman interaction frequencies with the external
133 field is smaller than or comparable to the scalar-coupling constant, 2πJ₁₂, between them. When the
134 strong coupling regime is achieved, the zero-quantum part of the scalar coupling, given by the operator
135 { $\hat{I}_{1+}\hat{I}_{2-} + \hat{I}_{1-}\hat{I}_{2+}$ }, becomes active, giving rise to flips and flops of spins I₁ and I₂. The couplings to the
136 third spin S, J₁₃ and J₂₃, are assumed to be unequal (otherwise coupling to the proton give rise to an
137 identical shift of the NMR frequencies of spins 1 and 2 and does not modify the eigenstates of this
138 subsystem). The Hamiltonian of the spin system can be written as follows (in ħ units):



$$\hat{\mathcal{H}}_{CCH} = \omega_1 \hat{I}_{1z} - \omega_2 \hat{I}_{2z} - \omega_3 \hat{S}_z + 2\pi J_{12}(\hat{\mathbf{I}}_1 \cdot \hat{\mathbf{I}}_2) + 2\pi J_{13} \hat{I}_{1z} \hat{S}_z + 2\pi J_{23} \hat{I}_{2z} \hat{S}_z \quad (1)$$

139 Here $\hat{\mathbf{I}}_1$, $\hat{\mathbf{I}}_2$ and $\hat{\mathbf{S}}$ are the spin operators; ω_1 , ω_2 and ω_3 stand for the NMR frequencies of the
 140 corresponding nuclei. We assume that the heteronucleus S is coupled weakly to I spins due to the large
 141 difference in their NMR frequencies, i.e., $|\omega_1 - \omega_3|, |\omega_2 - \omega_3| \gg |\omega_1 - \omega_2|, 2\pi J_{13}, 2\pi J_{23}$, and keep only
 142 the secular part of the heteronuclear coupling Hamiltonian.

143 In the present case, the nuclear magnetic number, m_S , of spin S is a “good quantum number”, which is
 144 conserved because \hat{S}_z commutes with the Hamiltonian. For this reason, it is possible to find the solution
 145 for the spin dynamics of spins I_1 and I_2 for two separate cases, which corresponds to the two different
 146 values of m_S being $+\frac{1}{2}$ and $-\frac{1}{2}$, i.e., spin S is in the “spin-up” $|\alpha\rangle$ state or “spin-down” $|\beta\rangle$ state. In each
 147 case, the Hamiltonian of the carbon subsystem is as follows:

$$\hat{\mathcal{H}}_{CC} = -\{\omega_1 - 2\pi J_{13} S_z\} \hat{I}_{1z} - \{\omega_2 - 2\pi J_{23} S_z\} \hat{I}_{2z} + 2\pi J_{12}(\hat{\mathbf{I}}_1 \cdot \hat{\mathbf{I}}_2) \quad (2)$$

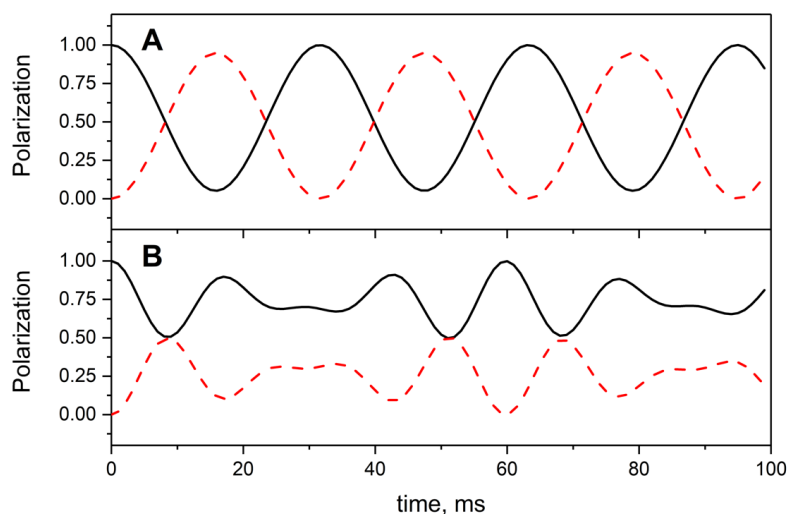
148 Hence, in the Hamiltonian given by eq. (1) we replace the \hat{S}_z operator by the m_S value, which is $\pm \frac{1}{2}$. Hence,
 149 the $\delta\omega$ value is modified and it depends on the m_S value:

$$\delta\omega_{\pm} = \{\omega_1 - \omega_2\} \mp \pi\{J_{13} - J_{23}\} = \delta\omega \mp \pi \cdot \delta J \quad (3)$$

150 The eigenstates of the subsystem of spin 1 and spin 2 are

$$\begin{aligned} |1\rangle &= |\alpha\alpha\rangle, \quad |2\rangle_{\pm} = \cos\theta_{\pm} |\alpha\beta\rangle + \sin\theta_{\pm} |\beta\alpha\rangle \\ |3\rangle_{\pm} &= -\sin\theta_{\pm} |\alpha\beta\rangle + \cos\theta_{\pm} |\beta\alpha\rangle, \quad |4\rangle = |\beta\beta\rangle \end{aligned} \quad (4)$$

151 Here the “mixing angle” is given by the values of $\delta\omega_{\pm}$ and J_{12} : $\tan 2\theta_{\pm} = 2\pi J_{12}/\delta\omega_{\pm}$. When $\delta\omega_{\pm}$
 152 approaches zero, the mixing angle goes to $\frac{\pi}{4}$ meaning that the eigenstates become singlet and triplet
 153 states: the spins are strongly coupled. When $\delta\omega_{\pm}$ is much greater than the coupling, the eigenstates are
 154 obviously the Zeeman states.



155
 156 **Figure 3.** Polarization transfer among two strongly coupled nuclei (a) in the absence and (b) in the presence (bottom)
 157 of a heteronucleus. Here, we present the time dependence of $\langle I_{1z} \rangle$ (black solid lines) and $\langle I_{2z} \rangle$ (red dashed lines),
 158 normalized to the initial value of $\langle I_{1z} \rangle$. The density operator at time $t = 0$ is $\sigma_0 = \hat{I}_{1z}$. Parameters of the simulation
 159 were $\delta\omega/2\pi = 10$ Hz, $J_{12} = 30$ Hz, and (a) $\delta J = 0$ Hz and (b) $\delta J = 100$ Hz.



160 Even in this simple system, it is clear that the condition $|\omega_1 - \omega_2| \ll 2\pi J_{12}$ is not sufficient to guarantee
 161 strong coupling of the two carbons. Indeed, when δJ is greater than $\delta\omega$ and $2\pi J_{12}$ the carbon spins
 162 become weakly coupled in the two sub-ensembles, corresponding to $m_S = \pm \frac{1}{2}$.

163 How do heteronuclear couplings affect polarization transfer in the carbon system? We assume that at $t =$
 164 0 one of the spins has polarization $\langle I_{1z} \rangle = P_0$ and the other spin is not polarized, $\langle I_{2z} \rangle = 0$. Hereafter, it
 165 is convenient to use normalization $P_0 = 1$. The state of the spin system is then given by the density
 166 operator

$$\sigma_0 = \hat{I}_{1z} \quad (5)$$

167 As shown previously (Ivanov et al., 2006), in the two-spin system of I_1 and I_2 , in the absence of coupling
 168 to any other spin, the polarization evolves with time as follows:

$$\langle I_{1z} \rangle(t) = 1 - \sin^2 \theta \frac{1 - \cos[\omega_{ZQC} t]}{2}, \quad \langle I_{2z} \rangle(t) = \sin^2 \theta \frac{1 - \cos[\omega_{ZQC} t]}{2} \quad (6)$$

169 where $\tan 2\theta = 2\pi J_{12}/\delta\omega$ and the oscillation frequency $\omega_{ZQC} = \sqrt{\delta\omega^2 + (2\pi J_{12})^2}$ is the frequency of
 170 the ZQC between the eigenstates $|2\rangle$ and $|3\rangle$. Hence, coherent exchange of polarization is taking place.
 171 As $\delta\omega$ becomes smaller the frequency of the oscillations decreases, but the amplitude increases: at $\delta\omega \rightarrow$
 172 0 we obtain $\omega_{ZQC} = 2\pi|J_{12}|$ and complete exchange is possible when $t = 1/(2J_{12})$.

173 In the presence of scalar couplings to the third spin S , here a proton (I_1 and I_2 are carbon-13 nuclei), the
 174 expressions should be modified: the evolution should be calculated for each specific spin state of the
 175 proton, $|\alpha\rangle$ and $|\beta\rangle$, and sum of the two curves should be taken. We obtain at the following expression:

$$\begin{aligned} \langle I_{1z} \rangle(t) &= 1 - \sin^2 \theta_+ \frac{1 - \cos[\omega_{ZQC}^+ t]}{4} - \sin^2 \theta_- \frac{1 - \cos[\omega_{ZQC}^- t]}{4} \\ \langle I_{2z} \rangle(t) &= \sin^2 \theta_+ \frac{1 - \cos[\omega_{ZQC}^+ t]}{4} + \sin^2 \theta_- \frac{1 - \cos[\omega_{ZQC}^- t]}{4} \end{aligned} \quad (7)$$

176 where the evolution frequencies are equal to $\omega_{ZQC}^\pm = \sqrt{\delta\omega_\pm^2 + (2\pi J_{12})^2}$.

177 The time dependence of the expectation value for the longitudinal polarizations of spins I_1 and I_2 is
 178 presented in **Figure 3** in the presence and the absence of scalar couplings to a heteronucleus. In the
 179 absence of heteronuclear coupling the two strongly coupled spins (the strong coupling condition is
 180 fulfilled since $2\pi J_{12} > \delta\omega$) almost completely exchange polarizations. The polarization transfer is of a
 181 coherent nature and the frequency of the oscillations is close to the scalar-coupling constant J_{12} . In the
 182 presence of different heteronuclear scalar couplings to the third spin S , the time-evolution changes
 183 considerably. The two spins are no longer in the regime of strong coupling, since $|\delta\omega_\pm| > 2\pi J_{12}$. The
 184 efficiency of polarization transfer is reduced and complete exchange of polarization is no longer possible.
 185 The time dependence also becomes more complex: instead of a single frequency ω_{ZQC} found in the
 186 previous case, here two frequencies appear: ω_{ZQC}^+ and ω_{ZQC}^- . Hence, when couplings to heteronuclei are
 187 present, the condition $\delta\omega \sim 2\pi J_{12}$ does not guarantee that the homonuclei are in the strong-coupling
 188 regime.

189 These results show that the interaction with a heteronucleus clearly alters polarization transfer in strongly
 190 coupled networks. Consequently, we expect strong effects of heteronuclear interactions on polarization
 191 transfers in systems with several heteronuclei. Notably, we anticipate that polarization transfer among
 192 strongly coupled carbon spins will be dramatically different in the presence of proton decoupling, which
 193 effectively removes proton-carbon spin-spin interactions.

194 B. Spin dynamics simulations



195 In addition to this simple model, we carried out numerical simulations in a realistic multi-spin system: the
 196 isopropyl group of carbon-13 labeled leucine. This spin system contains three carbon-13 nuclei I_1 , I_2 , and
 197 I_3 : the C^γ carbon-13 and the two C^δ carbon-13 nuclei. In addition, the spin system includes seven protons
 198 S_j : each C^δ nucleus is coupled to the three protons of the methyl group, and the C^γ carbon-13 nucleus is
 199 coupled to one proton. We model the effects of fast field variation and coherent spin dynamics at low
 200 field. We consider two cases, namely, polarization transfer in the presence and in the absence of proton
 201 decoupling.

202 The simulation method is as follows. The semi-selective inversion pulse on spin I_3 generates the initial
 203 density operator for the three-spin I system:

$$\sigma_0 = \sigma(t=0) = \hat{I}_{1z} + \hat{I}_{2z} - \hat{I}_{3z} \quad (8)$$

204 Hence, we generate a population difference for the states $|\alpha\alpha\beta\rangle$, $|\alpha\beta\alpha\rangle$ and $|\beta\alpha\alpha\rangle$: the first state is
 205 overpopulated, while the other two states are underpopulated. The three-spin system under study, C^γ ,
 206 $C^{\delta 1}$ and $C^{\delta 2}$, has a LAC at $B = B_{LAC} \approx 1.1$ T, see [Figure 4](#). Upon passage through a LAC during the field
 207 jump $B_{HF} \rightarrow B_{LF}$ due to the sample shuttle transfer, the population difference is expected to be
 208 converted into a coherence between the states, which have the LAC: these adiabatic states correspond
 209 to the $|\alpha\alpha\beta\rangle$ and $|\alpha\beta\alpha\rangle$ states at high fields. To calculate the actual spin state at $B = B_{LF}$ we solve
 210 numerically the Liouville-von Neumann equation for the spin density operator

$$\frac{d}{dt}\sigma = -i[\hat{\mathcal{H}}(t), \sigma] \quad (9)$$

211 The Hamiltonian of the spin system at a magnetic field B is as follows:

$$\begin{aligned} \hat{\mathcal{H}}(B) = & -\gamma_C B \sum_{i=1}^3 (1 + \delta_{Ci}) \hat{I}_{iz} - \gamma_H B \sum_{j=1}^7 (1 + \delta_{Hj}) \hat{S}_{jz} + 2\pi \sum_{i \neq k} J_{Cik} (\hat{\mathbf{I}}_i \cdot \hat{\mathbf{I}}_k) \\ & + 2\pi \sum_{j \neq m} J_{Hjm} (\hat{\mathbf{S}}_j \cdot \hat{\mathbf{S}}_m) + 2\pi \sum_{i=1}^3 \sum_{j=1}^7 J'_{ij} \hat{I}_{iz} \hat{S}_{jz} \end{aligned} \quad (10)$$

212 Here γ_C and γ_H are the carbon and proton gyromagnetic ratios, δ_{Ci} and δ_{Hj} are the chemical shifts of the
 213 i -th carbon and j -th proton, J_{Cik} is the scalar coupling constant between the i -th and k -th carbon, J_{Hjm} is
 214 the scalar coupling constant between the j -th and m -th proton, J'_{ij} is the scalar coupling constant between
 215 the i -th carbon and j -th proton, $\hat{\mathbf{I}}_i$ and $\hat{\mathbf{S}}_j$ are the spin operator of the i -th carbon and j -th proton. Given
 216 the range of magnetic fields considered here, heteronuclear scalar couplings are considered to be weak.
 217 The precise values of the calculation parameters are given in [Table 1](#). Since the magnetic field B changes
 218 with time, the Hamiltonian $\hat{\mathcal{H}}$ is also time-dependent. In the calculation we consider three carbons and
 219 seven protons (six protons in three CH_3 -groups and the γ -proton). Using this Hamiltonian we evaluate the
 220 density operator after the first field jump, $\sigma(t = t_1)$. The Liouville-von Neumann equation is integrated
 221 using 1 ms time increments and assuming that for each step the Hamiltonian is constant, similarly to
 222 simulations carried out for relaxation experiments (Bolik-Coulon et al., 2020). In the calculation, we ignore
 223 relaxation effects, since the dimensionality of the relaxation superoperator is too big for the multi-spin
 224 system considered here and our focus is on coherent effects.

225 At $B = B_{LF}$ the density operator evolves under a constant Hamiltonian, at the end of the evolution period
 226 it becomes as follows:

$$\sigma(t_1 + \tau) = \exp(-i\hat{\mathcal{H}}(B_{LF})\tau) \sigma(t_1) \exp(i\hat{\mathcal{H}}(B_{LF})\tau) \quad (11)$$

227 The $B_{LF} \rightarrow B_{HF}$ field jump is simulated numerically in the same way as the first field jump (the time
 228 interval is split into many small steps). Finally, knowing the density operator σ_{fin} at $t = t_1 + \tau + t_2$, we



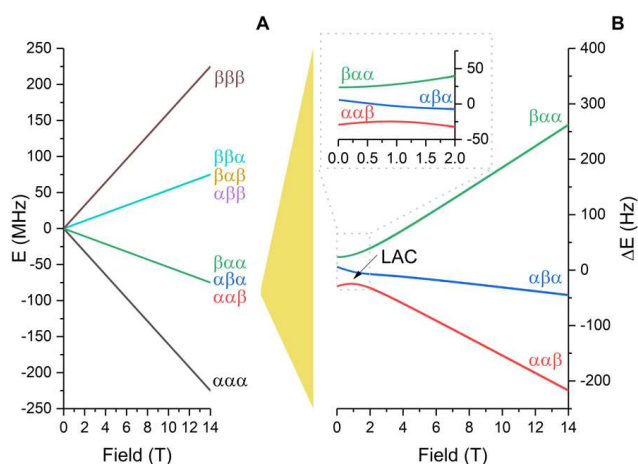
229 evaluate the NMR signals of the nuclei of interest as the expectation values of their z-magnetization
 230 $\langle I_{iz} \rangle = \text{Tr}\{\hat{I}_{iz}\sigma_{fin}\}$.

231

Table 1. Parameters used for energy calculations:

Chemical shifts	
C^γ	24.14 ppm
$C^{\delta 1}$	22.05 ppm
$C^{\delta 2}$	20.92 ppm
Scalar couplings	
$J(C^\gamma - C^{\delta 1})$	35 Hz
$J(C^\gamma - C^{\delta 2})$	35.4 Hz
$J(C^{\delta 1} - C^{\delta 2})$	0 Hz

232



233

234 **Figure 4.** (A) Energy levels of the $\{C^\gamma, C^{\delta 1}, C^{\delta 2}\}$ spin system at variable magnetic field strength in the absence of
 235 scalar coupling with protons. Levels are assigned at high field, where the spin system is weakly coupled. (B) energy
 236 levels, corresponding to the $\alpha\alpha\beta$ and $\alpha\beta\alpha$ states at high field, have a LAC at 1.1 T, which is responsible for generation
 237 of the zero quantum coherences. To visualize the energy levels better, in the right panels we have subtracted the
 238 large Zeeman energy from the actual energy and show the energy difference. The calculation is done using
 239 parameters listed in **Table 1** and neglecting carbon-proton couplings.

240 The method used for modelling the experiments with decoupling at $B = B_{LF}$ is different. After evaluating
 241 the density operator $\sigma(t = t_1)$ we trace out the proton degree of freedom and define the density
 242 operator of the carbon subsystem as $\sigma_C(t_1) = \text{Tr}_H\{\sigma(t_1)\}$, with the argument that proton polarization is
 243 destroyed by decoupling. The partial trace procedure implies that when $\sigma_{ik,jl}$ is a proton-carbon density
 244 operator (in the notation of spin states i, j stand for the proton states and k, l stand for the carbon states),
 245 the elements of the carbon density operator are: $\{\sigma_C\}_{k,l} = \sum_i \sigma_{ik,il}$. One should note that proton two-
 246 spin operators may contain a zero-quantum component, which would stand proton decoupling.
 247 Consideration of effects of such coherences is beyond the scope of this work: we expect this to only lead
 248 to small perturbations of the observed behavior. Then we introduce the Hamiltonian of the carbon
 249 subsystem

$$\hat{\mathcal{H}}_C(B_{LF}) = -\gamma_C B_{LF} \sum_{i=1}^3 (1 + \delta_{Ci}) \hat{I}_{iz} + 2\pi \sum_{i \neq k} J_{Cik} (\hat{\mathbf{I}}_i \cdot \hat{\mathbf{I}}_k) \quad (12)$$



250 Using this Hamiltonian, we evaluate the density operator of the ^{13}C spins at the end of the evolution period
 251 as follows

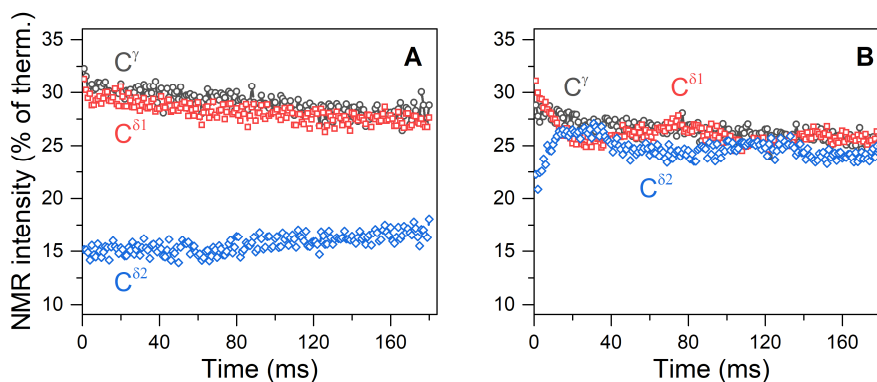
$$\sigma_C(t_1 + \tau) = \exp(-i\hat{\mathcal{H}}_C(B_{LF})\tau) \sigma_C(t_1) \exp(i\hat{\mathcal{H}}_C(B_{LF})\tau) \quad (13)$$

252 The final step in evaluating the ZQC evolution is introducing the carbon-proton density operator. This is
 253 done by multiplying $\sigma_C(t_1 + \tau)$ and the density operator of non-polarized protons (as decoupling removes
 254 any proton spin order). Hence

$$\sigma(t_1 + \tau) = \sigma_C(t_1 + \tau) \otimes \sigma_H^{dec}, \quad \sigma_H^{dec} = \frac{1}{2^7} \prod_{j=1}^7 \hat{1} \quad (14)$$

255 where $\hat{1}$ is a 2×2 unity matrix. The final step of the calculation, the field jump $B_{LF} \rightarrow B_{HF}$, is modelled
 256 in the same way as in the previous case.

257 Finally, we would like to comment on the $B(t)$ dependence, which was used in calculation. The distance
 258 dependence of the magnetic field $B(z)$ is precisely known but the precise $z(t)$ is not known. We modelled
 259 this dependence assuming that motion goes with a constant speed (in experiments, constant-speed
 260 motion is achieved after a 5-10 ms lag delay for acceleration). Non-ideal agreement between theory and
 261 experiment can be attributed to the fact that the precise $z(t)$ dependence is not known (our previous
 262 works show that the knowledge of $z(t)$ is required for modeling).



263
 264 **Figure 5.** Observed τ -dependence of the polarizations of carbon-13 nuclei C^γ , $C^{\delta 1}$ and $C^{\delta 2}$ measured (A) without ^1H
 265 decoupling, and (B) with ^1H decoupling. The NMR intensities are plotted in percent of the intensities of the NMR
 266 signals in the 150.9 MHz ^{13}C spectra (i.e., at 14.1 T) at thermal equilibrium.

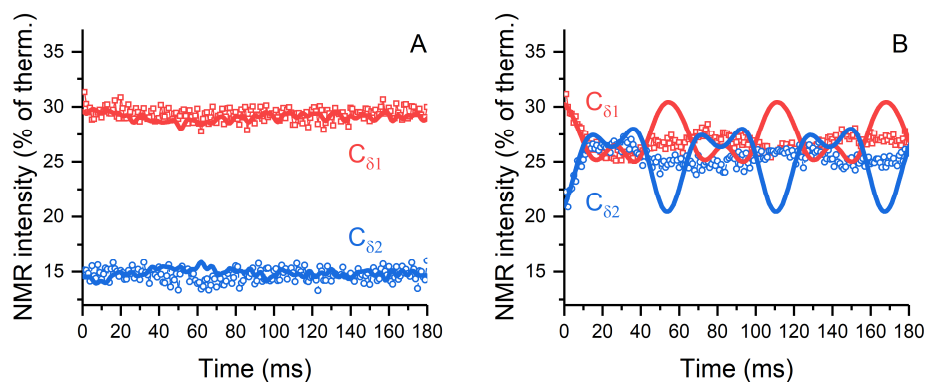
267 IV. Results and discussion

268 The experimental τ -dependences of the measured spin polarization are shown in **Figure 5**. One can see
 269 that without decoupling no coherent behavior is found: polarization simply decays due to relaxation and
 270 no coherent oscillations are visible (**Figure 5A**). In the presence of proton decoupling the situation is
 271 drastically different: coherent oscillations are clearly observed, which mediate polarization exchange
 272 between the $C^{\delta 1}$ and $C^{\delta 2}$ nuclei. We attribute such polarization exchange to the ZQC, which is generated
 273 by passage through the LAC. The coherence gives rise to exchange of the populations of the two states,
 274 which experience the LAC. These levels are correlated with the $|\alpha\alpha\rangle$ and $|\alpha\beta\rangle$ high-field states. Hence,
 275 polarization transfer gives rise to population exchange of the states $|\alpha\alpha\rangle$ (initially overpopulated state)
 276 and $|\alpha\beta\rangle$ (initially underpopulated state). As a result, the state of the first spin, C^γ , does not change, but
 277 the other two spins, $C^{\delta 1}$ and $C^{\delta 2}$, exchange polarizations. With the available speed and range of the field-
 278 cycling, other coherences are not excited, i.e., non-adiabatic variation of the Hamiltonian is achieved only
 279 for the pairs of levels that have the LAC in between B_{LF} and B_{HF} , i.e., only the LAC shown in **Figure 4**
 280 contributes to spin mixing. The C^γ spin never shows any oscillatory polarization transfer, which is an



281 indication that the specific LAC is responsible for the observed effect. In conclusion, a zero-quantum
282 coherence of the two carbon-13 nuclei $C^{\delta 1}$ and $C^{\delta 2}$ is excited by fast magnetic field jump between 14.1 T
283 and 0.33 T.

284 The oscillatory behavior does not show up in the absence of proton decoupling. There are two reasons
285 for that. First, the multiple proton-carbon couplings give rise to a set of ZQC frequencies, instead of a
286 unique frequency in the presence of decoupling. Second and more importantly, proton-carbon-13
287 couplings prevent the carbon subsystem from reaching the strong-coupling regime. Thus, the amplitude
288 of coherent evolutions is drastically reduced (see Eq. 7) and becomes negligible (Fig. 5.A). As a result, in
289 experiments without decoupling the ZQC decays because of inhomogeneous broadening of the ZQC
290 evolution frequency, *i.e.* relaxation. We would like to stress that the ZQC of interest is excited by the field
291 jump, which is identical for experiments with and without proton decoupling at low field. However, the
292 ZQC does not reveal itself and does not give rise to efficient polarization transfer in the experiment
293 without decoupling.



294
295 **Figure 6.** Calculated τ -dependence of polarization (lines) overlaid with the observed time traces (points) obtained
296 (A) without ^1H decoupling, and (B) with ^1H decoupling. The slowly relaxing background (compare with the data shown
297 in [Figure 5](#)) has been subtracted from the time traces, to enable comparison between theory and simulations.
298 Observed NMR intensities are normalized to intensities in 150.9 MHz (14.1 T) ^{13}C spectra at thermal equilibrium. We
299 use the subtraction procedure because relaxation effects were not taken into account in the calculation;
300 consequently, we are unable to consider polarization decay due to relaxation at B_{LF} and during the field variation.
301 To enable comparison of the experiment and calculation results, the amplitude of oscillations in polarization transfer
302 traces were scaled with the same factor, then the starting polarization values were adjusted individually to give best
303 agreement with experimental data.

304 These considerations are confirmed by theoretical modeling ([Figure 6](#)). In the presence of carbon-proton
305 couplings coherent oscillations are hardly observed: only fast oscillations of very small amplitude can be
306 seen in the simulated curves. By contrast, in the absence of the proton-carbon couplings, *i.e.*, when
307 decoupling is used, coherent evolutions become manifest with slower oscillations of larger amplitude. The
308 results of numerical modeling are in good agreement with the experimental data. As relaxation effects
309 are not taken into account in simulations, to ease comparison we subtracted the slowly relaxing
310 background from the experimental time traces. In addition, we rescaled all calculated traces with the
311 same factor; then the starting polarization values were adjusted individually to achieve the best
312 agreement with the experimental data. Such a data treatment becomes necessary because relaxation is
313 active not only during spin mixing at the B_{LF} field, but also during the field jumps. The agreement between
314 the experimental data and simulation in [Figure 6](#) is not ideal, possibly because some small long-range
315 scalar couplings are not included in the simulation but most likely because the field switching profile is
316 not known exactly: previous studies of the spin dynamics in field-cycling NMR experiments (Pravdivtsev
317 et al., 2013; Kiryutin et al., 2013) suggest that using the precise $B(t)$ profile is crucial for simulating
318 coherent polarization transfer phenomena.



319 The absence of strong-coupling regime, in spite of scalar coupling constants larger than the difference in
320 Larmor frequencies is somewhat counterintuitive but clearly explained when taking into account the
321 effect of large heteronuclear scalar couplings (Eqs. 2-4). In the present case, the effect is even more
322 pronounced since the two δ carbon-13 nuclei of leucine are coupled to no less than 3 protons each, further
323 splitting resonance frequencies in the absence of proton decoupling. A conventional way to present the
324 weak coupling regime consists in stating that the part of the scalar coupling Hamiltonian (Eq. 1) that is
325 proportional to a zero-quantum product operator is non-secular in the frame of the Zeeman interactions
326 of the two coupled spins, which is true if the scalar coupling constant is much smaller than the difference
327 in Larmor frequencies of the two spins. Here, the weak-coupling regime is extended because this zero-
328 quantum part can be considered non-secular in the interaction frame of the heteronuclear scalar
329 couplings (note that the perturbative treatment is allowed to the extent that the heteronuclear coupling
330 constants are much larger than the homonuclear coupling).

331 A particular consequence of the observation we report here can be relevant for experiments where the
332 strong scalar-coupling regime is created by radio-frequency irradiation: isotropic mixing for total
333 correlation spectroscopy (TOCSY) (Braunschweiler and Ernst, 1983). We have recently introduced a two-
334 field TOCSY experiment where isotropic mixing is carried out at 0.33 T and chemical shift evolutions occur
335 at high field (Kadeřávek et al., 2017), which makes broadband carbon-13 TOCSY straightforward. This
336 study included a control experiment where no radio-frequency pulses were applied at low field (see Figure
337 3.b in reference (Kadeřávek et al., 2017). Intuitively, one would have expected cross-peaks to be observed
338 for carbon-13 nuclei in strongly-coupled networks at 0.33 T. Some cross peaks could indeed be observed
339 within the aliphatic carbon region of leucine and in the aromatic ring of phenylalanine. The current
340 investigation suggests that strong scalar couplings between carbon-13 nuclei are less prevalent than
341 expected at 0.33 T. The observed cross-peaks were possibly due to cross relaxation and not necessarily
342 coherent evolution under strong scalar couplings. Conventional TOCSY experiments might also be altered
343 by the effect of large heteronuclear scalar couplings. In this case, isotropic mixing sequences have been
344 optimized on isolated pairs of two coupled spins (Kadkhodaie et al., 1991), excluding the effects of scalar
345 couplings to heteronuclei or as heteronuclear decoupling sequences that happen to be efficient at
346 isotropic mixing (Rucker and Shaka, 1989; Shaka et al., 1988). Although isotropic mixing sequences
347 decouple heteronuclear scalar couplings, optimizing simultaneously for homo- and heteronuclear scalar
348 coupling operators may improve homonuclear coherence transfers.

349 **V. Conclusions**

350 In this work, we present a study of coherent polarization transfer in a system of (strongly) coupled ^{13}C
351 nuclei. Spin coherences are zero-quantum coherences, which are generated by a fast non-adiabatic
352 magnetic field jump. Such coherences are excited most efficiently when the system goes through a LAC
353 during the field switch. Here we indeed pass through a LAC in a system of three coupled ^{13}C spins and
354 investigate the spin dynamics at low fields, where strong couplings of the carbon spins are expected.

355 We can clearly demonstrate the polarization transfer in the carbon-13 spin subsystem is strongly affected
356 by spin-spin interactions with the protons in the molecule. In this situation, the role of these interactions
357 can be determined by comparing the experiments with and without proton decoupling at low fields. When
358 decoupling is used, we observe coherent polarization exchange between two of the three carbons: such
359 a behavior is typical when the spin coherences are excited upon non-adiabatic passage through a specific
360 LAC. In the absence of decoupling, i.e., when heteronuclear interactions are present, we cannot observe
361 such a behavior: polarization transfer is very inefficient and coherent phenomena are not found. We
362 attribute this to the fact that relatively strong proton-carbon couplings (i) drive the carbon system away
363 from the strong coupling condition and (ii) give rise to a set of evolution frequencies instead of a unique
364 ZQC frequency. These considerations are supported by an analytical model of a three-spin system and
365 numerical simulations in a multi-spin system.



366 Our results are of importance for analyzing polarization transfer phenomena at low magnetic fields and
367 for interpreting NMR data obtained under apparent strong coupling conditions. Under such conditions
368 heteronuclear spin-spin interactions might disturb “strong coupling” of homonuclei and substantially alter
369 spin dynamics.

370 Acknowledgements

371 This work has been supported by the Russian Foundation for Basic Research (grants Nos. 19-29-10028 and
372 19-33-90251). I.V.Z. acknowledges support from the French embassy in the Russian Federation, in the
373 framework of the Ostrogradsky fellowship (project No. 933824A).

374 References

- 375 Appelt, S., Häsing, F. W., Sieling, U., Gordji-Nejad, A., Glöggler, S., and Blümich, B.: Paths from Weak to
376 Strong Coupling in NMR, *Phys. Rev. A*, 81, 023420, <https://doi.org/10.1103/PhysRevA.81.023420>, 2010.
- 377 Blanchard, J. W., and Budker, D.: Zero- to Ultralow-Field NMR, *eMagRes*, 5, 1395-1409,
378 <https://doi.org/10.1002/9780470034590.emrstm1369>, 2016.
- 379 Bodenhausen, G., Freeman, R., Morris, G. A., and Turner, D. L.: Proton-Coupled Carbon-13 J Spectra in the
380 Presence of Strong Coupling. II, *J. Magn. Reson.*, 28, 17-28, [https://doi.org/10.1016/0022-2364\(77\)90252-](https://doi.org/10.1016/0022-2364(77)90252-9)
381 9, 1977.
- 382 Bolik-Coulon, N., Kaderavek, P., Pelupessy, P., Dumez, J. N., Ferrage, F., and Cousin, S. F.: Theoretical and
383 Computational Framework for the Analysis of the Relaxation Properties of Arbitrary Spin Systems.
384 Application to High-Resolution Relaxometry, *J. Magn. Reson.*, 313,
385 <https://doi.org/10.1016/j.jmr.2020.106718>, 2020.
- 386 Braunschweiler, L., and Ernst, R. R.: Coherence Transfer by Isotropic Mixing - Application to Proton
387 Correlation Spectroscopy, *J. Magn. Reson.*, 53, 521-528, [https://doi.org/10.1016/0022-2364\(83\)90226-3](https://doi.org/10.1016/0022-2364(83)90226-3),
388 1983.
- 389 Bryant, R. G., and Korb, J. P.: Nuclear Magnetic Resonance and Spin Relaxation in Biological Systems,
390 *Magn. Reson. Imaging*, 23, 167-173, <https://doi.org/10.1016/j.mri.2004.11.026>, 2005.
- 391 Cavanagh, J.: *Protein NMR Spectroscopy : Principles and Practice*, 2nd ed., Academic Press, Amsterdam;
392 Boston, XXV, 885 p. pp., 2007.
- 393 Charlier, C., Khan, S. N., Marquardsen, T., Pelupessy, P., Reiss, V., Sakellariou, D., Bodenhausen, G.,
394 Engelke, F., and Ferrage, F.: Nanosecond Time Scale Motions in Proteins Revealed by High-Resolution NMR
395 Relaxometry, *J. Am. Chem. Soc.*, 135, 18665-18672, <https://doi.org/10.1021/ja409820g>, 2013.
- 396 Chou, C.-Y., Chu, M., Chang, C.-F., Yu, T., Huang, T.-H., and Sakellariou, D.: High Sensitivity High-Resolution
397 Full Range Relaxometry Using a Fast Mechanical Sample Shuttling Device and a Cryo-Probe, *J. Biomol.*
398 *NMR*, 66, 187-194, <https://doi.org/10.1007/s10858-016-0066-5>, 2016.
- 399 Chou, C.-Y., Abdesslem, M., Bouzigues, C., Chu, M., Guiga, A., Huang, T.-H., Ferrage, F., Gacoin, T.,
400 Alexandrou, A., and Sakellariou, D.: Ultra-Wide Range Field-Dependent Measurements of the Relaxivity
401 of Gd_{1-x}Eu_xVO₄ Nanoparticle Contrast Agents Using a Mechanical Sample-Shuttling Relaxometer, *Sci. Rep.*,
402 7, 44770, <https://doi.org/10.1038/srep44770>, 2017.
- 403 Cousin, S. F., Charlier, C., Kaderavek, P., Marquardsen, T., Tyburn, J. M., Bovier, P. A., Ulzega, S., Speck, T.,
404 Wilhelm, D., Engelke, F., Maas, W., Sakellariou, D., Bodenhausen, G., Pelupessy, P., and Ferrage, F.: High-
405 Resolution Two-Field Nuclear Magnetic Resonance Spectroscopy, *Phys. Chem. Chem. Phys.*, 18, 33187-
406 33194, <https://doi.org/10.1039/c6cp05422f>, 2016a.
- 407 Cousin, S. F., Kaderavek, P., Haddou, B., Charlier, C., Marquardsen, T., Tyburn, J. M., Bovier, P. A., Engelke,
408 F., Maas, W., Bodenhausen, G., Pelupessy, P., and Ferrage, F.: Recovering Invisible Signals by Two-Field
409 NMR Spectroscopy, *Angew. Chem., Int. Edit.*, 55, 9886-9889, <https://doi.org/10.1002/anie.201602978>,
410 2016b.
- 411 Ernst, R. R., Bodenhausen, G., and Wokaun, A.: *Principles of Nuclear Magnetic Resonance in One and Two*
412 *Dimensions*, The International Series of Monographs on Chemistry, 14, Clarendon Press; Oxford University
413 Press, Oxford Oxfordshire, New York, 1987.



- 414 Foroozandeh, M., Adams, R. W., Meharry, N. J., Jeannerat, D., Nilsson, M., and Morris, G. A.: Ultrahigh-
415 Resolution NMR Spectroscopy, *Angew. Chem., Int. Edit.*, 53, 6990-6992,
416 <https://doi.org/10.1002/anie.201404111>, 2014.
- 417 Geen, H., and Freeman, R.: Band-Selective Radiofrequency Pulses, *J. Magn. Reson.*, 93, 93-141,
418 [https://doi.org/10.1016/0022-2364\(91\)90034-Q](https://doi.org/10.1016/0022-2364(91)90034-Q), 1991.
- 419 Goddard, Y., Korb, J.-P., and Bryant, R. G.: The Magnetic Field and Temperature Dependences of Proton
420 Spin-Lattice Relaxation in Proteins, *J. Chem. Phys.*, 126, 175105, <https://doi.org/10.1063/1.2727464>,
421 2007.
- 422 Grootveld, M., Percival, B., Gibson, M., Osman, Y., Edgar, M., Molinari, M., Mather, M. L., Casanova, F.,
423 and Wilson, P. B.: Progress in Low-Field Benchtop NMR Spectroscopy in Chemical and Biochemical
424 Analysis, *Anal. Chim. Acta*, 1067, 11-30, <https://doi.org/10.1016/j.aca.2019.02.026>, 2019.
- 425 Ivanov, K. L., Miesel, K., Yurkovskaya, A. V., Korchak, S. E., Kiryutin, A. S., and Vieth, H.-M.: Transfer of
426 CIDNP among Coupled Spins at Low Magnetic Field, *Appl. Magn. Reson.*, 30, 513-534,
427 <https://doi.org/10.1007/Bf03166215>, 2006.
- 428 Ivanov, K. L., Yurkovskaya, A. V., and Vieth, H.-M.: Coherent Transfer of Hyperpolarization in Coupled Spin
429 Systems at Variable Magnetic Field, *J. Chem. Phys.*, 128, 154701, <https://doi.org/10.1063/1.2901019>,
430 2008.
- 431 Ivanov, K. L., Pravdivtsev, A. N., Yurkovskaya, A. V., Vieth, H.-M., and Kaptein, R.: The Role of Level Anti-
432 Crossings in Nuclear Spin Hyperpolarization, *Prog. Nucl. Mag. Res. Sp.*, 81, 1-36,
433 <https://doi.org/10.1016/j.pnmrs.2014.06.001>, 2014.
- 434 Kadeřávek, P., Strouk, L., Cousin, S. F., Charlier, C., Bodenhausen, G., Marquardsen, T., Tyburn, J. M.,
435 Bovier, P. A., Engelke, F., Maas, W., and Ferrage, F.: Full Correlations across Broad NMR Spectra by Two-
436 Field Total Correlation Spectroscopy, *ChemPhysChem*, 18, 2772-2776,
437 <https://doi.org/10.1002/cphc.201700369>, 2017.
- 438 Kadkhodaie, M., Rivas, O., Tan, M., Mohebbi, A., and Shaka, A. J.: Broad-Band Homonuclear Cross
439 Polarization Using Flip-Flop Spectroscopy, *J. Magn. Reson.*, 91, 437-443, [https://doi.org/10.1016/0022-2364\(91\)90210-K](https://doi.org/10.1016/0022-2364(91)90210-K), 1991.
- 441 Keeler, J.: *Understanding NMR Spectroscopy*, Wiley, Chichester, England; Hoboken, NJ, XV, 459 p. pp.,
442 2005.
- 443 Kiryutin, A. S., Yurkovskaya, A. V., Kaptein, R., Vieth, H.-M., and Ivanov, K. L.: Evidence for Coherent
444 Transfer of Para-Hydrogen-Induced Polarization at Low Magnetic Fields, *J. Phys. Chem. Lett.*, 4, 2514-
445 2519, <https://doi.org/10.1021/jz401210m>, 2013.
- 446 Kiryutin, A. S., Pravdivtsev, A. N., Ivanov, K. L., Grishin, Y. A., Vieth, H.-M., and Yurkovskaya, A. V.: A Fast
447 Field-Cycling Device for High-Resolution NMR: Design and Application to Spin Relaxation and
448 Hyperpolarization Experiments, *J. Magn. Reson.*, 263, 79-91, <https://doi.org/10.1016/j.jmr.2015.11.017>,
449 2016.
- 450 Korchak, S. E., Ivanov, K. L., Pravdivtsev, A. N., Yurkovskaya, A. V., Kaptein, R., and Vieth, H.-M.: High
451 Resolution NMR Study of T_1 Magnetic Relaxation Dispersion. III. Influence of Spin 1/2 Hetero-Nuclei on
452 Spin Relaxation and Polarization Transfer among Strongly Coupled Protons, *J. Chem. Phys.*, 137, 094503,
453 <https://doi.org/10.1063/1.4746780>, 2012.
- 454 Ledbetter, M. P., Theis, T., Blanchard, J. W., Ring, H., Ganssle, P., Appelt, S., Blümich, B., Pines, A., and
455 Budker, D.: Near-Zero-Field Nuclear Magnetic Resonance, *Phys. Rev. Lett.*, 107, 107601,
456 <https://doi.org/10.1103/PhysRevLett.107.107601>, 2011.
- 457 Levitt, M. H.: *Spin Dynamics : Basics of Nuclear Magnetic Resonance-2nd Ed.*, 2008.
- 458 Miesel, K., Ivanov, K. L., Yurkovskaya, A. V., and Vieth, H.-M.: Coherence Transfer During Field-Cycling NMR
459 Experiments, *Chem. Phys. Lett.*, 425, 71-76, <https://doi.org/10.1016/j.cplett.2006.05.025>, 2006.
- 460 Pfändler, P., and Bodenhausen, G.: Strong Coupling Effects in Z-Filtered Two-Dimensional NMR
461 Correlation Spectra, *J. Magn. Reson.*, 72, 475-492, [https://doi.org/10.1016/0022-2364\(87\)90152-1](https://doi.org/10.1016/0022-2364(87)90152-1), 1987.
- 462 Pravdivtsev, A. N., Yurkovskaya, A. V., Kaptein, R., Miesel, K., Vieth, H.-M., and Ivanov, K. L.: Exploiting
463 Level Anti-Crossings for Efficient and Selective Transfer of Hyperpolarization in Coupled Nuclear Spin
464 Systems, *Phys. Chem. Chem. Phys.*, 15, 14660-14669, <https://doi.org/10.1039/c3cp52026a>, 2013.
- 465 Redfield, A. G.: High-Resolution NMR Field-Cycling Device for Full-Range Relaxation and Structural Studies
466 of Biopolymers on a Shared Commercial Instrument, *J. Biomol. NMR*, 52, 159-177,
467 <https://doi.org/10.1007/s10858-011-9594-1>, 2012.



- 468 Roberts, M. F., and Redfield, A. G.: High-Resolution ^{31}P Field Cycling NMR as a Probe of Phospholipid
469 Dynamics, *J. Am. Chem. Soc.*, 126, 13765-13777, <https://doi.org/10.1021/ja046658k>, 2004a.
- 470 Roberts, M. F., and Redfield, A. G.: Phospholipid Bilayer Surface Configuration Probed Quantitatively by
471 ^{31}P Field-Cycling NMR, *P. Natl. Acad. Sci. USA.*, 101, 17066-17071, <https://doi.org/10.1007/s10858-011->
472 9594-1, 2004b.
- 473 Rucker, S. P., and Shaka, A. J.: Broad-Band Homonuclear Cross Polarization in 2D NMR Using DIPSI-2, *Mol.*
474 *Phys.*, 68, 509-517, <https://doi.org/10.1080/00268978900102331>, 1989.
- 475 Shaka, A. J., Keeler, J., Frenkiel, T., and Freeman, R.: An Improved Sequence for Broad-Band Decoupling -
476 WALTZ-16, *J. Magn. Reson.*, 52, 335-338, [https://doi.org/10.1016/0022-2364\(83\)90207-X](https://doi.org/10.1016/0022-2364(83)90207-X), 1983.
- 477 Shaka, A. J., Lee, C. J., and Pines, A.: Iterative Schemes for Bilinear Operators - Application to Spin
478 Decoupling, *J. Magn. Reson.*, 77, 274-293, [https://doi.org/10.1016/0022-2364\(88\)90178-3](https://doi.org/10.1016/0022-2364(88)90178-3), 1988.
- 479 Tayler, M. C. D., Theis, T., Sjolander, T. F., Blanchard, J. W., Kentner, A., Pustelny, S., Pines, A., and Budker,
480 D.: Invited Review Article: Instrumentation for Nuclear Magnetic Resonance in Zero and Ultralow
481 Magnetic Field, *Rev. Sci. Instrum.*, 88, 091101, <https://doi.org/10.1063/1.5003347>, 2017.
- 482 Vallurupalli, P., Scott, L., Williamson, J. R., and Kay, L. E.: Strong Coupling Effects During X-Pulse CPMG
483 Experiments Recorded on Heteronuclear ABX Spin Systems: Artifacts and a Simple Solution, *J. Biomol.*
484 *NMR*, 38, 41-46, <https://doi.org/10.1007/s10858-006-9139-1>, 2007.
- 485 Wagner, S., Dinesen, T. R. J., Rayner, T., and Bryant, R. G.: High-Resolution Magnetic Relaxation Dispersion
486 Measurements of Solute Spin Probes Using a Dual-Magnet System, *J. Magn. Reson.*, 140, 172-178,
487 <https://doi.org/10.1006/jmre.1999.1811>, 1999.
- 488 Zhukov, I. V., Kiryutin, A. S., Yurkovskaya, A. V., Grishin, Y. A., Vieth, H.-M., and Ivanov, K. L.: Field-Cycling
489 NMR Experiments in Ultra-Wide Magnetic Field Range: Relaxation and Coherent Polarization Transfer,
490 *Phys. Chem. Chem. Phys.*, 20, 12396-12405, <https://doi.org/10.1039/C7CP08529J>, 2018.